DAMAGE REPAIR VERSUS AGING IN BIOFILMS

Running title: Damage repair versus aging in biofilms

Robyn J. Wright,[a,b,c#] Robert J. Clegg,[b,d] Timothy L. R. Coker,[b,e] Jan-Ulrich Kreft[b]

[a] School of Life Sciences, University of Warwick, Coventry, UK

[b] School of Biosciences & Institute of Microbiology and Infection (IMI) & Centre for Computational Biology (CCB), University of Birmingham, Birmingham, UK

[c] School for Resource and Environmental Studies, Dalhousie University, Halifax, Nova Scotia, Canada

[d] Tessella, 26 The Quadrant, Abingdon, Oxfordshire, UK

[e] Cancer Research UK, 2 Redman Place, London E20 1JQ

[#] Address correspondence to Robyn J. Wright, robyn.wright@dal.ca; robyn-wright@hotmail.com.

Word counts

Abstract: 250

Importance: 146

Main text: 5456

ORCID

RW: 0000-0003-0562-2610

RC: 0000-0001-7041-9745

TC: 0000-0002-2516-0639

JUK: 0000-0002-2351-224X

Author contributions

JUK and RJC initially designed the study with later input from RJW and TLRC. All simulations and analyses shown were carried out by RJW with guidance from RJC and JUK. TLRC performed preliminary simulation experiments to choose many of the simulation parameters. RJW and JUK wrote the first draft of the manuscript and all authors contributed to revisions. The authors declare no conflicts of interest.

Acknowledgements

RJW and TLRC were supported by BBSRC, UK; RW *via* a Midlands Integrative Biosciences Training Partnership PhD scholarship and TLRC *via* a University of Warwick Systems Biology Doctoral Training Centre PhD scholarship. RJC and JUK are grateful to the UK National Centre for the Replacement, Refinement & Reduction of Animals in Research (NC3Rs) for funding their development of individual-based models (IBMs) for the gut environment (eGUT grant NC/K000683/1). The funders had no role in study design, data collection and interpretation, or the decision to submit the work for publication.

ABSTRACT

The extent of senescence due to damage accumulation (or aging) is evidently evolvable as it varies hugely between species and is not universal, suggesting that its fitness advantages depend on life history and environment. In contrast, repair of damage is present in all organisms studied. Repair and segregation of damage have not always been considered as alternatives, despite the fundamental trade-off between investing resources into repair or growth. For unicellular organisms, unrepaired damage could be divided asymmetrically between daughter cells, leading to aging of one and rejuvenation of the other. Repair of unicells has been shown to be advantageous in well-mixed environments such as chemostats. However, most microorganisms live in spatially structured systems such as biofilms with gradients of environmental conditions and cellular physiology as well as clonal population structure. We asked whether this clonal structure might favor aging by damage segregation as this can be seen as a division of labor strategy, akin to the germline soma division in multicellular organisms. We used an individual-based model with a newly developed adaptive repair strategy where cells respond to their current intracellular damage levels by investing into repair machinery accordingly. We found that the new adaptive repair strategy was advantageous whenever efficient and optimal, both in biofilms and chemostats. Thus, biofilms do not favor a germline soma-like division of labor between daughter cells in terms of damage segregation. We suggest that damage segregation is only beneficial when active and effective, extrinsic mortality is high and a degree of multicellularity is present.

IMPORTANCE

Damage is an inevitable consequence of life, leading to a trade-off between allocating resources into damage repair or into growth whilst allowing aging, *i.e.*, segregation of damage upon cell division. Few studies considered repair as an alternative to aging. Moreover, all previous studies merely considered well-mixed environments, although the vast majority of unicellular organisms live in spatially structured environments, exemplified by biofilms, and fitness advantages in well-mixed systems often turn into disadvantages in spatially structured systems. We compared the fitness consequences of aging versus damage repair in biofilms with an individual-based model implementing an adaptive repair mechanism based on sensing damage. We found that aging is not beneficial. Instead, it is useful as a stress response to deal with damage that failed to be repaired when (i) clearly asymmetric cell division is feasible; (ii) extrinsic mortality is high; and (iii) a degree of multicellularity is present.

KEYWORDS

Evolution, division of labor, mathematical modelling, ageing, senescence, trade-offs

INTRODUCTION

Senescence is all around us, yet it is not obvious why it has evolved in many taxa as it would appear to be detrimental to the fitness of individuals. Importantly, the extent of senescence, manifesting in decreasing fecundity and/or increasing mortality with age, is clearly evolvable as it varies hugely between species and is *not* universal. For example, several taxa of simple multicellular organisms can fully regenerate and for several taxa of complex multicellular organisms, fecundity does not simply decrease with age and/or mortality does not simply increase with age (1–3). An evolutionary explanation for the various extents of senescence present in different organisms is challenging, particularly for unicellular organisms that divide apparently symmetrically, such as most prokaryotes and some eukaryotic unicells, in contrast to multicellular animals with a clear division of labor between germline and soma (4, 5). However, the first single-cell study of division asymmetry in *Escherichia coli* highlighted that morphological symmetry does not exclude functional asymmetry as daughter cells inheriting the old cell pole were shown to grow a little slower than the mother cell while the new cell pole daughters grew a little faster (6). Ironically, *Caulobacter crescentus*, the bacterium first studied in terms of aging (7), as it has substantial morphological and functional asymmetry in cell division, has been shown in more recent high-throughput microfluidic studies to maintain a constant growth rate over cell divisions under benign conditions (8) and to divide protein aggregates symmetrically between mother and daughter cells (9).

Following the first single-cell studies that suggested the existence of aging in unicellular prokaryotes (7, 10, 11) and unicellular eukaryotes (12), there has been a gold rush of studies eager to demonstrate aging in further unicells, such as bacteria (13–15) and eukaryotic algae (16–19). However, the loss of fecundity (10) or increase of mortality (20) with age,

97 demonstrated in some of these unicells, are rather small effects compared with the resource
98 limitations of growth and high external mortality in most environments. The effects are also
99 much smaller than in the budding yeast, which has long been known to have a limited
100 replicative lifespan (21), supported by several recent high-throughput single-cell studies (22–
101 28). However, it may be misleading to regard the budding yeast as a unicellular organism as
102 wild relatives are capable of dimorphic growth (29) and domesticated strains rapidly evolve
103 multicellularity (30, 31). Crucially, a number of recent experimental results have led to a
104 reinterpretation of aging, primarily in the sense of segregating protein aggregates, as a stress
105 response rather than an evolved characteristic of growth under benign conditions (9, 20, 32–
106 38).
107
108 In concert with the gold rush for experimental evidence for aging, there has also been one of
109 mathematical modelling studies eager to find evolutionary advantages of aging. Some of these
110 models did not consider extrinsic mortality (39–41), although it favors rapid and early
111 reproduction and thus tilts the evolutionary trade-off towards investment of resources into
112 growth and reproduction, rather than maintenance and repair (1, 42). Some also did not
113 consider repair as an alternative (40, 41, 43, 44) or did not consider the cost of repair (39).
114
115 Repair is present in all organisms studied and evidence for the evolution of mechanisms that
116 repair damage, such as misfolded and aggregated proteins (9), is beyond doubt. Of the few
117 models that consider both extrinsic mortality and costly repair, the model of Ackermann *et al.*
118 (2007) (45) was the first. It found that asymmetric damage segregation outperformed repair.
119 In contrast, our previous study, Clegg *et al.* (2014) (46), found that repair was always
120 beneficial, while damage segregation was beneficial only in addition to repair and if three

121 conditions were fulfilled simultaneously: (i) damage is toxic, (ii) damage accumulates at a high
122 rate and (iii) repair is inefficient. The reason for this discrepancy could be pinned down. In
123 Ackermann *et al.* (2007) (45), rather than growing, cells divide at fixed time intervals, while in
124 Clegg *et al.* (2014) (46), cells grow by consuming substrate and divide when they have reached
125 a threshold size. This enabled both an immediate benefit of repair (increased growth rate of
126 a less damaged cell leading to earlier division) and an immediate cost of repair (diverting
127 resources away from growth to repair machinery). Overall, this made repair advantageous.
128
129 More recent models that also consider repair have come to similar conclusions (36, 47, 48).
130 Vedel *et al.* (2016) (36), in particular, has advanced our understanding with an experimentally
131 validated model that considers the fitness of the whole lineage. This helped to identify a
132 positive feedback loop, shifting growing lineages towards less damaged cells and explaining
133 how higher stress levels lead to higher damage accumulation which in turn leads to higher
134 damage segregation.
135
136 None of these studies considered the fitness effects of aging and repair in spatially structured
137 environments such as biofilms, although biofilms are prevalent in nature and important for
138 ecosystem function. For humans, they have many advantages in biotechnology but also cause
139 big problems in industry and health. Biofilms are heterogeneous in both time and space (49)
140 and cells that are growing within them are therefore exposed to varying, and often limiting,
141 nutrient regimes (50). This leads to gradients in growth rate and the presence of an active
142 layer in biofilms, where active growth only occurs close to the boundary of the biofilm, due to
143 slow nutrient diffusion (51). Growth within biofilms has also been shown to confer tolerance
144 to damage-inducing agents, such as antibiotics (49, 52–54) and UV radiation (55, 56), and it is

145 therefore likely that these gradients of growth rate and stress could make the evolutionary
146 benefits of aging and repair different from spatially uniform environments, such as
147 chemostats. Moreover, biofilms have a clonal population structure unless the cells remain
148 motile (57–59). This can have strong effects on the evolution of division of labor (60). Damage
149 segregation can be seen as a division of labor akin to the germline soma differentiation in
150 multicellular animals (61). Thus, we hypothesized that biofilms might favor damage
151 segregation over repair.
152
153 To test this hypothesis, we developed a new individual-based model with adaptive repair,
154 whereby cells were able to sense and respond to their current intracellular damage levels.
155 This enables an appropriate response to gradients of stress and damage in biofilms. We found
156 that adaptive repair rather than damage segregation or a fixed rate of repair was the optimal
157 strategy for unicells growing in a biofilm, but only when the rate of damage accumulation was
158 proportional to the cells' specific growth rate.

RESULTS

Characteristics of adaptive repair. We developed a new repair strategy where allocation of newly synthesized protein into repair machinery, denoted by $\hat{\beta}$, rather than growth machinery, depends on the current level of damage in the cell and compared this with previous strategies (Fig. 1). The idea was that the cell can sense and appropriately respond to its damage level. This adaptive repair is more appropriate than a fixed repair strategy when rates of growth and damage accumulation vary in time or space, *e.g.* in fluctuating or spatially structured environments, such as biofilms. Adaptive repair is therefore meant to replace the previous strategy of a fixed allocation into repair machinery at an optimal level, β, which is appropriate for constant or chemostat environments, where growth and damage accumulation rates are in a steady state, like in our previous study, Clegg *et al.* (2014) (46). There, we estimated the optimal, fixed investment into repair (here simply referred to as fixed repair) by examining the mean specific growth rates of cells with different investments into repair and found that for a damage accumulation rate of 0.1 h^{-1}, an investment into repair of $\beta = 0.07$ was optimal for both asymmetric and symmetric strategies (for the case where damage is toxic, that we focus on here). The purpose of this section is to examine the consequences of the new adaptive repair strategy and to test whether it is equivalent to the previous optimal repair strategy in steady state environments.

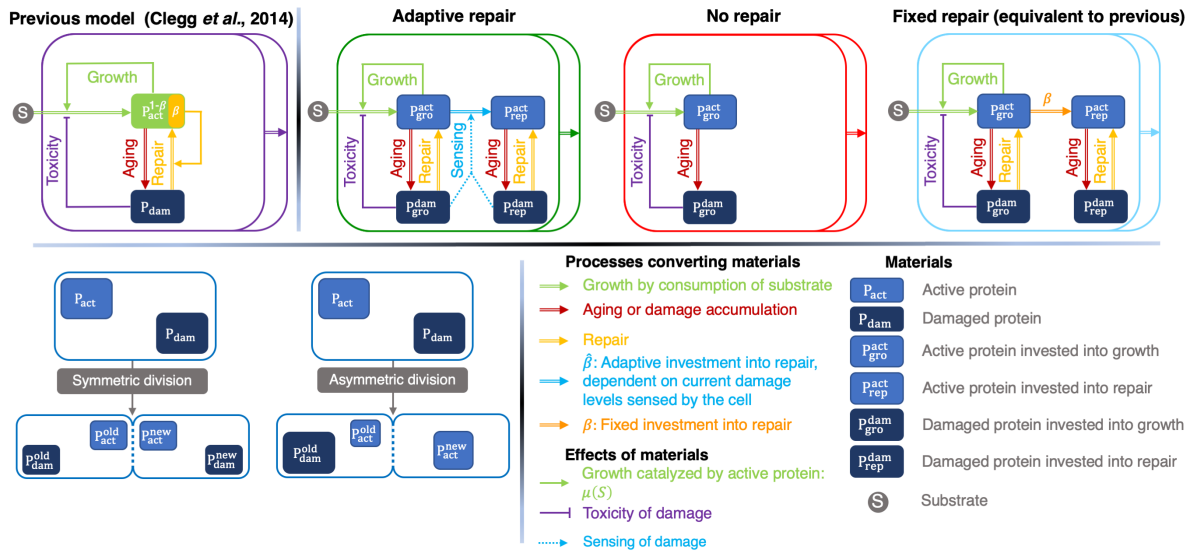

FIG 1 General schematic of division and repair strategies used in this study, giving rise to 6 combinations: (i) symmetric division with no repair (NR) (ii) symmetric division with fixed repair (FR); (iii) symmetric division with adaptive repair (AR); (iv) asymmetric division (damage segregation) without repair (DS); (v) asymmetric division with fixed repair (DSFR); and (vi) asymmetric division with adaptive repair (DSAR).

178

179 **Consequences of adaptive repair on the fraction of repair protein in single cells.** The adaptive
180 repair strategy leads to an allocation into repair that responds to current levels of damage and
181 therefore lags behind the ideal level of repair machinery, unless damage levels reach a steady
182 state due to symmetric division (Fig. S1). Since asymmetric division causes sudden changes in
183 damage levels, the current investment into repair tracks the changing damage levels (Fig. 2A).
184 Damage levels then change as a result of repair, which in turn changes allocation into repair.
185 As a result, the level of repair machinery never reaches ideal levels in asymmetrically dividing
186 cells, in contrast to symmetrically dividing cells (Fig. 2A and S1). To approach ideal levels of
187 repair machinery more quickly, a high turnover of repair protein would be required. Since
188 cellular proteins that are not involved in regulation have a long half-life of more than one
189 generation (62), it seems more realistic to assume that repair protein does not turn over;
190 turnover would also be costly and unnecessary. Investment into repair varies greatly over the
191 cell cycle for cells with asymmetric segregation of damage but is always at approximately the

same level immediately before division. The investment into repair immediately before division is approximately the same as the fixed optimal investment into repair.

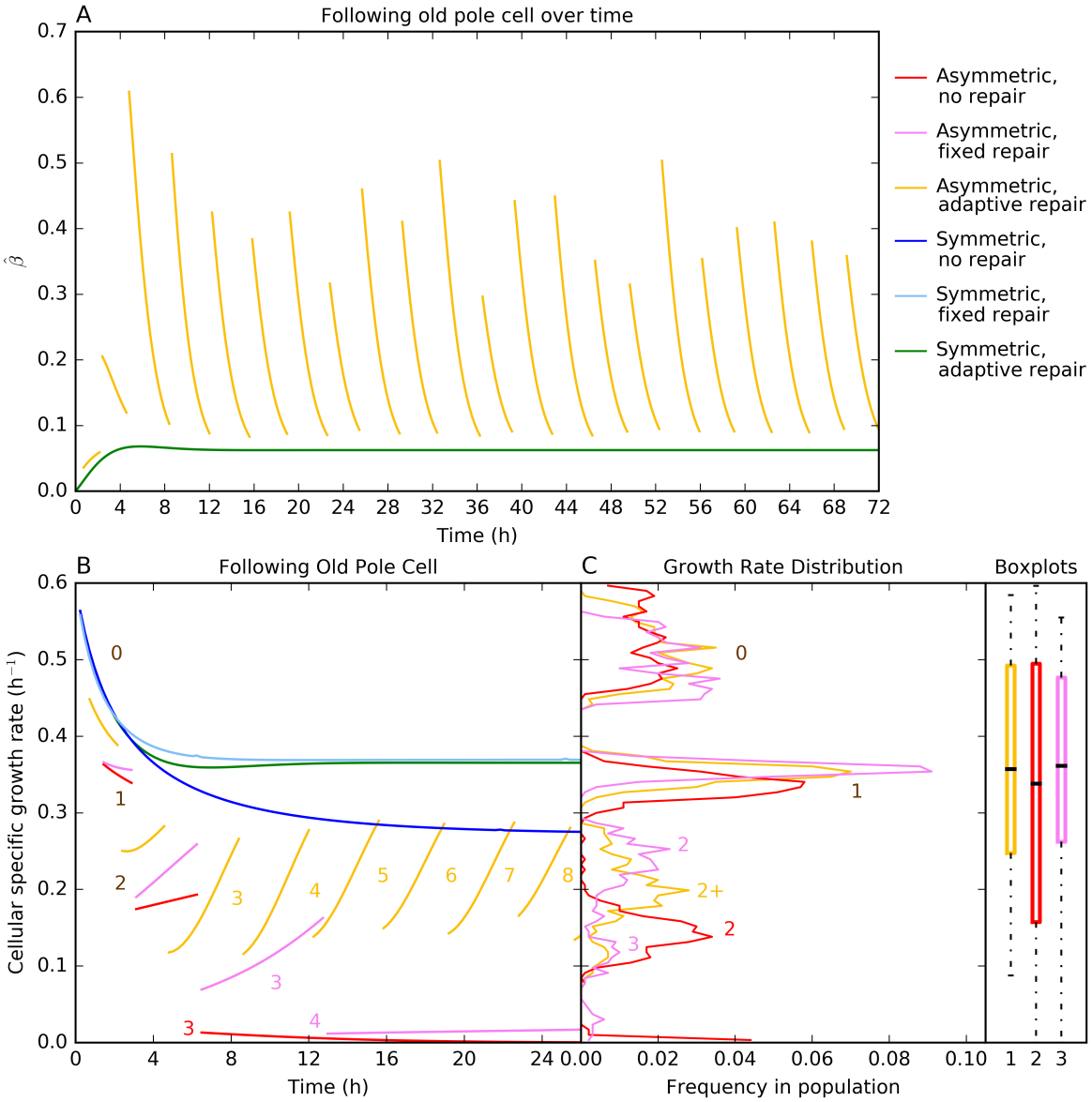

FIG 2 Characteristics of strategies in a constant environment (no competition). **(A)** Investment into repair ($\hat{\beta}$ on the y axis) for the new adaptive repair strategy following the old pole cell over many divisions. In asymmetric divisions, the old pole cell inherits all damage, leading to a jump in allocation into repair following division and then decreasing steadily until the next division. In symmetric divisions, damage, and therefore investment into repair, reaches a steady state. **(B)** Specific growth rate of a single cell over consecutive cell divisions. Numbers in the panel label generations and each generation is shown with a new line (for asymmetric strategies). The specific growth rate of an asymmetrically dividing cell with no repair (red, β = 0) drops quickly to zero. For a cell with fixed optimal repair (magenta, β = 0.07), it decreases more slowly over time but also reaches zero. For a cell

with adaptive repair (yellow, $\hat{\beta}$ variable), it decreases only initially towards a see saw pattern, as in (A). Specific growth rates do not change at division for symmetric strategies (blue, cyan, and green) and there is no difference between daughter cells. Symmetric strategies show an initial decrease in specific growth rate before reaching a steady state, with similar values for fixed and adaptive repair and lower without repair. **(C)** Distribution of specific growth rates in populations at steady state (snapshot taken at 100 days) for asymmetrically dividing cells. Specific growth rates of cells with adaptive repair are between those with fixed repair and those without repair. The medians and inter-quartile ranges for adaptive and fixed repair are close and higher than for symmetrically dividing cells. Data are reproduced with permission from Fig. 4A,B in (46), with the new adaptive repair strategy added. Specific growth rate was 0.6 h^{-1} and aging rate was 0.22 and dependent upon specific growth rate for all strategies. Replicate simulations are similar, see Fig. S2.

Consequences of adaptive repair on growth rates of individual cells. For asymmetric strategies, cells with adaptive repair maintained the highest specific growth rate across consecutive divisions from approximately generation three onwards (Fig. 2B). Without any repair, specific growth rate declined rapidly towards zero. With fixed repair, specific growth rates likewise declined towards zero, albeit more slowly. For symmetric strategies, specific growth rates were similar for all strategies while damage levels were low. Later, cells with repair maintained substantially higher specific growth rates than cells without repair (Fig. 2B).

Consequences of adaptive repair on the population level. A comparison of age and total biomass for each cell in a population shows the distribution of the levels of damage and how close the cells are to division (division is triggered when cells reach total biomass threshold; Fig. S3). For asymmetric strategies, adaptive repairers did not reach the high damage levels (old ages) of other strategies. For symmetric strategies, adaptive repairers were marginally older than fixed repairers, but much younger than cells without repair. Growth rates in populations of asymmetrically dividing cells had a multimodal distribution with marked differences between generations (Fig. 2C). There were fewer cells with very high and very low specific growth rates in populations using either fixed or adaptive repair. The growth rate

distribution of the new adaptive repair strategy was in between the fixed and no repair strategies. The medians for each population confirm that the population specific growth rates were highest for cells using the fixed repair strategy, though the adaptive repair strategy was only slightly lower and showed less variation between cells (Fig. 2C). Symmetrically dividing cells all had the same specific growth rate as the single cells in Fig. 2B with the fixed repairers having a slight specific growth rate advantage again. In summary, the new adaptive repair strategy led to growth rates that were very similar to fixed repair at the population level, but on the individual level, there were fewer old cells.

Competitions of aging strategies in constant and chemostat environments. Competitions are unambiguous and unbiased ways to measure fitness holistically. In the constant environment, cells were removed at random, which modelled extrinsic mortality, and the strategy that was left at the end had won. In the chemostat environment, cells were likewise removed randomly, but they also competed for the substrate that entered the environment with a given rate. This means that lineages that produced fewer offspring per time at the current concentration of substrate were washed out. In other words, cells with the highest specific growth rate (as dependent on substrate concentration) will emerge as the winner (on average, as removal is stochastic). The damage segregation without repair strategy (DS) quickly lost against either repair strategies (FR and AR) in both environments (Fig. 3). The winner took much longer to emerge between the two repair strategies and there were large fluctuations in the biomass ratios over the course of the simulations. In the constant environment, fixed repairers (FR) had an advantage, whereas in the chemostat, the adaptive repairers (AR) won in the end. Hence, the new adaptive repair strategy was slightly fitter than the fixed repair strategy in those natural environments that are better approximated by chemostats than

237 constant environments, such as systems that are mixed on a reasonably short time scale and
238 that receive resource inputs and experience removal of biomass by various means. However,
239 more environments are spatially structured and are therefore better modelled by biofilms, so
240 we turn to these in the next section.
241

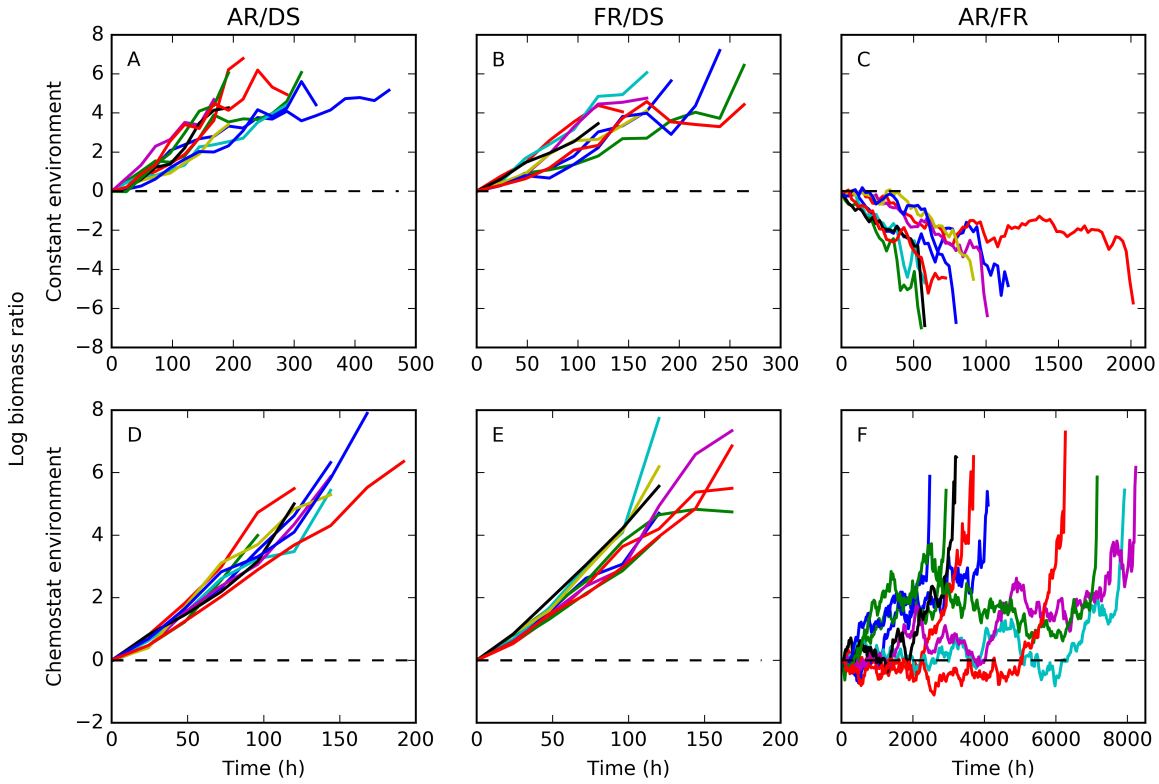

FIG 3 Pairwise competitions of aging strategies in constant and chemostat environments: Adaptive Repair without damage segregation (AR), Fixed optimal Repair without damage segregation (FR), Damage Segregation without repair (DS). Both repair strategies were substantially fitter than DS in either environment (A,B,D,E; n=10; proportion test, p=0.00195 for all). The two repair strategies were closer in fitness, as seen in Fig. 2B, and it took more than an order of magnitude longer before the final outcome was clear. FR was slightly fitter than AR in the constant environment (C; n=10; proportion test, p=0.00195), as expected from Fig. 2B, but not in the chemostat environment (F; n=10; proportion test, p=0.00195). Maximum specific growth rate was 0.6 h^{-1}, and aging rate was 0.22 h^{-1} and dependent upon specific growth rate for all strategies.

242

243 **Generating realistic biofilm structures in the absence of damage accumulation.** We first
244 identified which parameter set would give rise to typical, rough biofilm structures with 'finger'
245 formation (63–65), rather than flat biofilms, so that we could then study aging in biofilms using

246 realistic biofilm structures (Fig. S4 and File S1). These simulations were without aging or repair.
247 The substrate concentration in the bulk liquid was varied in order to change the dimensionless
248 group δ^2 that quantifies the extent to which biofilm growth is intrinsically limited (growth-
249 limited regime, high δ^2) or limited extrinsically by diffusional mass transport into the biofilm
250 (transport-limited regime, low δ^2; see Supplementary Materials and Methods for more
251 information on δ^2). Since biofilm roughness at the end of the simulations was not significantly
252 different between the three δ^2 regimes tested, we decided to continue our simulations with
253 only one value for δ^2; the intermediate value where $\delta^2 = 0.0069$.
254
255 **Biofilm simulations with constant damage accumulation rate.** For the biofilm simulations
256 with constant damage accumulation rate, we compared the asymmetric damage segregation
257 without repair (DS) and symmetric damage segregation with adaptive (AR) or fixed (FR) repair.
258
259 Repair of damaged material is assumed to require resources, *e.g.*, energy and some new
260 material to replace the damaged parts of the old material. These resources are assumed to be
261 supplied by endogenous metabolism of cellular material rather than the substrate, as the
262 latter is not always available. As a result, converting damaged material into undamaged, active
263 material comes at a loss of biomass (we assume a loss of 20% for reasons given in Clegg *et al.*
264 (2014) (46)). This loss leads to shrinking of cells (since the density of cells is assumed to be
265 constant), unless cells grow sufficiently fast to compensate, which is not the case in the lower
266 layers of a biofilm. Shrinking does not affect fitness in constant and chemostat environments
267 as only the numbers of organisms matters, but the shrinking of cells of the adaptive repair
268 strategy had profound effects on biofilm structure and reduced the fitness of this strategy in
269 biofilms (Fig. 4). In these competitions, the winner depended upon the initial cell density.

When the initial cell density was low, it appears that the winner depends more upon the initial, random placement; cells of any strategy that happen to be placed furthest away from the other strategies tend to win. When the initial cell density is higher, the winner is more dependent upon the fitness of that strategy. Because cells of the adaptive repair strategy shrink so much more than the other strategies, this effect is much greater for them.

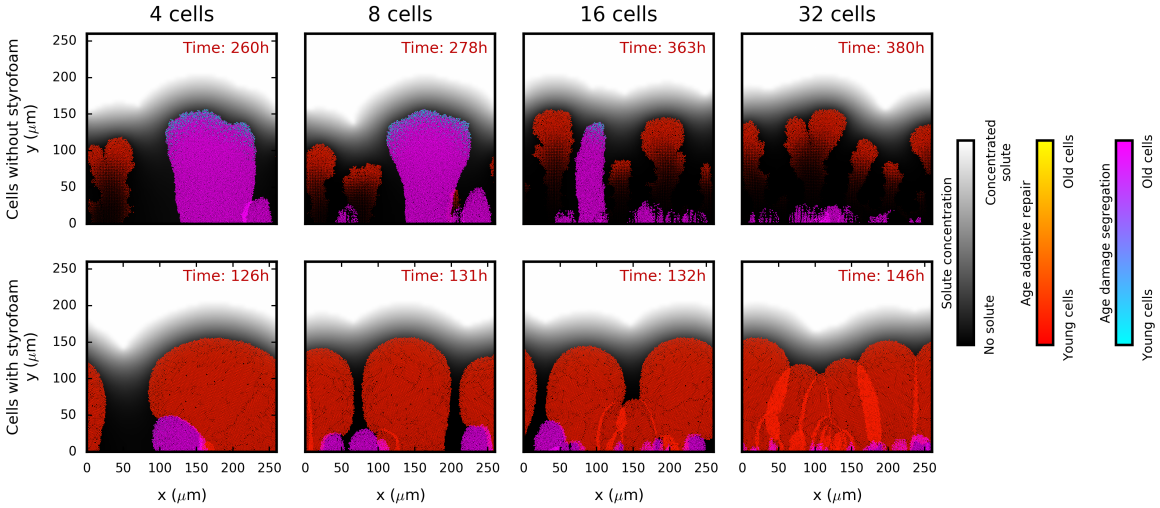

FIG 4 Damage segregation (DS, cold colors) *versus* adaptive repair (AR, warm colors) strategies in biofilms. Adaptive repairers are strongly affected by shrinking (top row) as they are much fitter when assumed not to shrink, *i.e.*, when the material lost due to repair is replaced with inert and massless material of the same volume ('styrofoam', bottom row). Initial cell density increases from left to right (4, 8, 16 or 32 cells). Biofilm structures shown have all reached a height of 154 μm. Cells are colored by age with different color gradients for each species. Maximum specific growth rate was 1.2 h^{-1} and damage accumulation rate was 0.1 h^{-1} (not proportional to specific growth rate) for all. Results of replicate simulations, simulations which competed DS and AR against the fixed optimal repair strategy (FR) and controls are shown in File S1. See Fig. S5 for time courses of log biomass ratios. For simulations without styrofoam, DS tended to be fitter than AR at initial densities of 4 and 8 cells, but AR was fitter at the higher initial densities of 16 and 32 cells (top row). For competitions between DS and FR, FR was fitter at densities of 8, 16 or 32 cells (File S1 and Fig. S5). In the simulations with 'styrofoam', AR and FR were always fitter than DS (bottom row; File S1 and Fig. S5). For competitions between AR and FR, FR was fitter in simulations without 'styrofoam', while AR was fitter in simulations with 'styrofoam'. Control simulations that competed two cells of the same strategy always led to no clear winner.

How much of the disadvantage of adaptive repairers was due to shrinking can be seen by comparing simulations with shrinking cells to identical simulations where, for the sake of

279 comparison, the lost material is assumed to continue to take up volume (*i.e.*, the lost material
280 has no mass but keeps its original volume, dubbed 'styrofoam'). In the simulations without
281 styrofoam, AR was only fitter than DS at initial densities of above 8 cells, FR was fitter than DS
282 at initial densities above 4 cells and FR was fitter than AR in all simulations. In the simulations
283 with styrofoam the results were much clearer; AR and FR are fitter than damage segregating
284 cells and AR was fitter than FR, regardless of the cell density at the beginning of the simulation
285 (Figs. 4 and S5).
286
287 The results caused by shrinking were thought to be unrealistic. Cells have not been observed
288 to shrink considerably, unless they have been starved for long periods of time, and biofilm
289 structures such as in Fig. 4 with a vanishing base due to endogenous metabolism have not, to
290 our knowledge, been observed, and would be mechanically unstable in the presence of shear
291 (66). Shrinking must therefore be either very limited in real cells, or the assumption that non-
292 growing cells accumulate damage at the same rate as rapidly growing cells must be wrong
293 (which would only cause the non-growing cells to shrink as the growing cells can make up the
294 lost volume). We decided to avoid this unrealistic shrinking by assuming that cells that do not
295 grow also do not accumulate damage. The damage accumulation rate was therefore assumed
296 to be proportional to cellular specific growth rate (and was matched to the previous damage
297 accumulation rate; Fig. S6), to allow for the very low rates of growth of cells below the active
298 layer of the biofilm (the active layer is shown in Fig. 5). This means that shrinking is not
299 abolished, but that slowly growing cells will accumulate damage and shrink at a lower rate as
300 repair, leading to shrinking, is less necessary. See Materials and Methods for further
301 explanation of this proportional damage accumulation rate. We therefore continued with a

damage accumulation rate of 0.22 that is dependent upon specific growth rate and also applied this to the earlier constant and chemostat environments.

AR performed better than FR in the biofilms with styrofoam (Fig. 4), and we therefore focus on the two main alternative strategies, AR and DS, in the following section.

Biofilm simulations where the damage accumulation rate is proportional to specific growth rate. When the damage accumulation rate was proportional to the specific growth rate, AR was more competitive than DS (Figs. 5 and 6; Fig. S7 also shows the controls). The higher the initial cell density, the stronger the advantage of AR and the earlier that they won. At the highest initial cell density (32 cells), AR won in all 50 replicate simulations (p=0.00). At the lowest cell density (4 cells), they won in the majority of the simulations (31 *vs* 19) but this difference was not statistically significant (p=0.119). The advantage of adaptive repair became statistically significant at initial cell densities of eight or higher (Table S1).

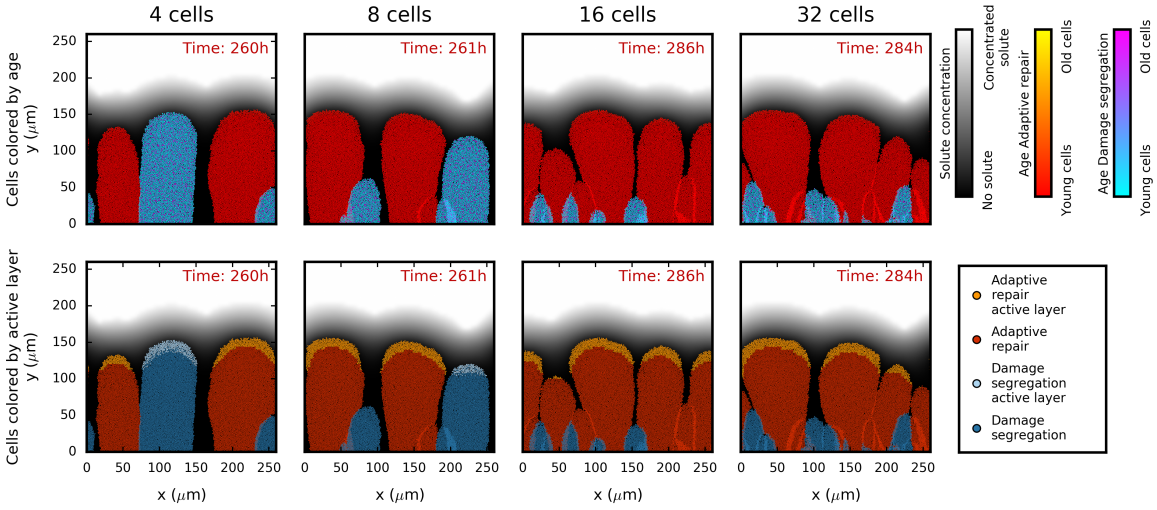

FIG 5 Damage segregation *versus* adaptive repair competitions in biofilms where damage accumulation rate is proportional to specific growth rate. From left to right, initial cell density increases (4, 8, 16 and 32 cells). Adaptive repair becomes more advantageous the

greater the initial cell density. In the top row, cells are colored by age, while in the bottom row, cells are colored brighter if they are in the active layer of rapidly growing cells, defined as cells with a specific growth rate within 5% of the highest at this time point. Biofilm structures shown have all reached a height of 154 μm. Maximum specific growth rate was 1.2 h^{-1} and damage accumulation rate was set at 0.22 h^{-1}. Repeat simulations are shown in File S1 and control competitions are shown alongside this figure in Fig. S7.

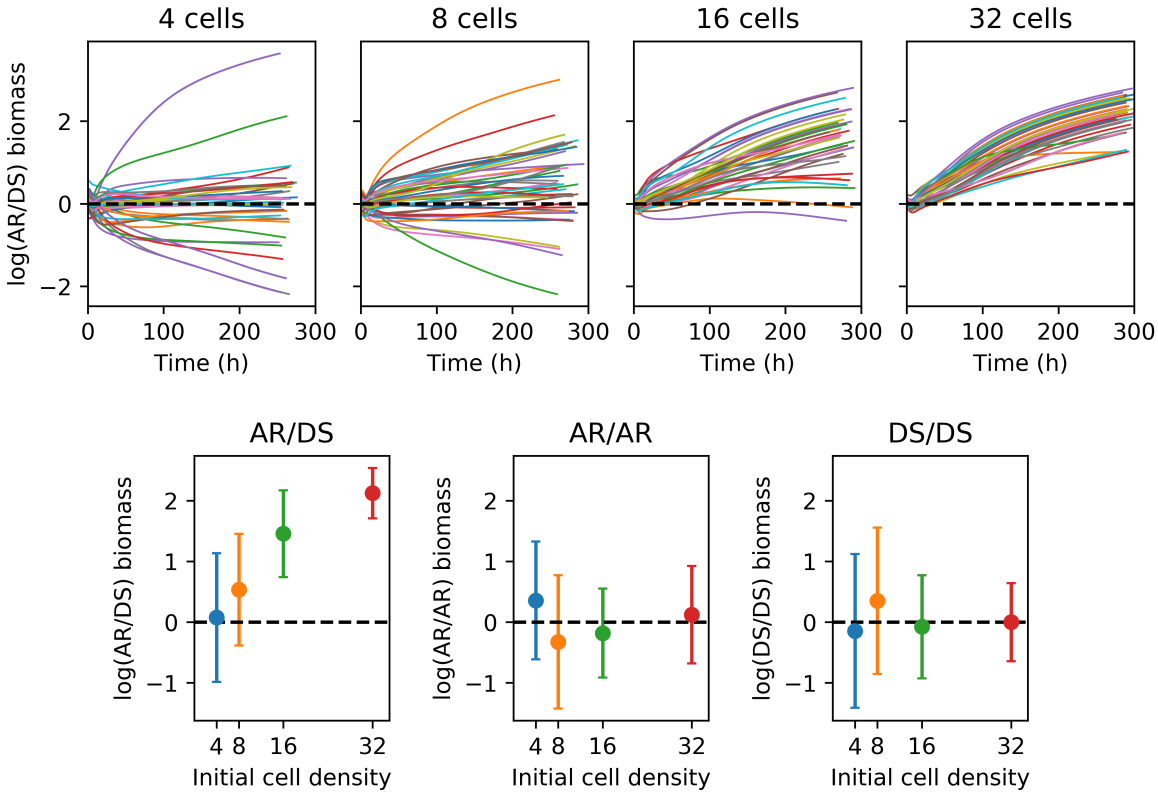

FIG 6 Time courses of log biomass ratios for 50 replicate biofilm competitions between adaptive repair (AR) and damage segregation (DS) strategies and their controls. Adaptive repair (AR) became the more advantageous the higher the initial cell density, compared with damage segregation (DS). At the start, 4, 8, 16 or 32 cells were randomly placed on the surface. Results are shown using log biomass ratios to make the horizontal line at log(ratio) = 0 (i.e., ratio = 1) a symmetry axis. The top row shows time courses for AR *versus* DS competitions, while the bottom row shows mean log(ratio)'s with standard deviations for all simulations, including controls, taken when biofilms had reached 154 μm (approximately 250 – 300 hours). Statistics for these competitions are shown in Table S1 and biofilm structures are plotted in Fig. 5 and File S1. Control time courses are shown in Fig. S7. Maximum specific growth rate was 1.2 h^{-1} and damage accumulation rate was set at 0.22 h^{-1} and dependent upon specific growth rate for all strategies.

We decided to use the log biomass ratios as the best measure of fitness after comparing the performance of a range of different metrics when both strategies were identical (controls in

Table S1 and Fig. S7). The ideal fitness measure should not be time-dependent, such that running simulations longer would not change outcomes. As the trends of the log biomass ratios in Figs. 6 and S7 show, using biomass at the end of the simulations (approximately 250 h) was appropriate since outcomes would not have changed had the simulations continued. Moreover, the fitness metric with its significance testing should never result in a statistically significant result when the two competitors were identical, as was the case with final growth rate (Table S1). Final growth rate was therefore not a suitable measure. Both biomass and population size could be used; they are strongly coupled, but the biomass changes are smoother than the cell numbers, hence, biomass was chosen as the fitness measure.

The biofilms formed from these equal mixtures of DS and AR, initially placed randomly on the substratum surface, show the spatial distribution of the strategies and the age and activity of the cells (Fig. 5 and S7). First, it can be seen that there was limited mixing of cells where neighboring 'fingers' touch (lines of different color standing out), consistent with our previous work (67, 68). This is due to the assumption that cells embedded in the biofilm matrix are not motile. Second, if finger-like cell clusters were similarly separated from other clusters, both strategies reached a similar height, suggesting that shrinking was negligible (Fig. 5; 4 cell initial density). This was despite repair leading to loss of material and cellular volume as growth could compensate for any losses when the rate of damage accumulation was proportional to growth rate. Third, the effect of increasing the initial cell density can also be seen. When there were only a few cells randomly placed on the substratum surface, it was likely that one cell happened to be further away from competing cells than any of the other cells. This lineage could therefore grow without much competition and became the highest finger producing the highest biomass, regardless of which strategy it followed. Hence, results at low cell density

were more dependent on the random initial cell positions determining the distance to competitors than on competitiveness. The higher the initial density, the less influenced the results were by the stochastic initial attachment of cells on the surface. In these cases, AR had the advantage. Finally, comparing the distribution of young *vs* old cells with the distribution of active *vs* inactive cells (Fig. 5) shows that AR were all young throughout the biofilm, while DS created a mixture of young (rejuvenated) and old (damage-keeping) cells throughout the cell clusters, regardless of height. Note that cells are only active when they are at the top of their biofilm finger and when this finger is at least about as high as the neighboring fingers because only then do they receive sufficient substrate diffusing in from the bulk liquid, which is separated from the biofilm by a concentration boundary layer (63–65). Hence, whether a strategy still had cells in the active layer was determined by whether it still had cells growing close to the maximum biofilm height, and not by how many cells it had that were very young.

DISCUSSION

Here, we investigated two alternative strategies for unicells to deal with intracellular damage: segregation or repair. Due to a trade-off between investing cellular resources into repair machinery *versus* growth machinery that is fundamental to all living organisms, repair is costly and therefore not obviously beneficial. This study is the first to compete these strategies in biofilms, representing spatially structured environments. We began by developing a new model for adaptive repair of cellular damage, whereby cells are able to sense and respond to current damage levels by investing into repair machinery accordingly, enabling cells to deal with spatial and temporal changes of conditions in biofilms. We found that in almost all conditions tested, adaptive repair was fitter than the asymmetric segregation of damage at division (Figs. 3 and 6). We also compared adaptive repair with our previous fixed optimal repair strategy (46) – in well-mixed environments where both strategies are suitable. Surprisingly, although cells with the adaptive repair mechanism had slightly lower growth rates than those with fixed optimal repair at the level of the individual (Fig. 2B), they outperformed them in the chemostat environment where there was competition for resources (Fig. 3). The likely reason for this is that with adaptive repair, there are more cells growing at the highest rate (Fig. 2C); as cells grow exponentially, any slight growth rate advantage will increase over time, resulting in a higher chance of division before stochastic removal from the chemostat.

When we initially applied the adaptive repair model to growth in biofilms we were surprised that the bases of biofilm 'fingers' of adaptive repairers were disappearing (Fig. 4). Since we assume that converting damaged into new material incurs a loss of 20% to account for the energy requirement of repair, the slowly growing cells at the base of the biofilm are not able

381 to compensate for this 20% loss of biomass due to repair with new growth. Therefore,
382 repairers shrink. This could be considered a biofilm specific disadvantage of repair. However,
383 we think such extensive shrinking is unrealistic. First, to our knowledge, extensive shrinking of
384 the volume of starving or dormant cells other than by cell division has not been observed and
385 this may be due to the murein sacculus maintaining cell shape. Second, these biofilm
386 structures with completely disappearing bases are not realistic as the slightest shear stress
387 would detach these structures (66, 69, 70). Moreover, one would expect that the higher the
388 rate of metabolism such as protein folding or respiratory electron transport, the higher the
389 chance of damage arising such as protein misfolding or damage by reactive oxygen species
390 (19, 71, 72). Indeed, organisms that grow more rapidly have been shown to also accumulate
391 damage more rapidly (47, 73) and can have a higher rate of mortality (38). Therefore, we
392 decided to make the simplest assumption that the rate of damage accumulation should be
393 proportional to the specific growth rate of individual cells. In this case, biofilm fingers of
394 adaptive repairers no longer had shrinking bases (Fig. 5) and now performed better than the
395 damage segregators (Fig. 6 and Table S1), as may be expected when cell death is
396 predominantly intrinsic rather than extrinsic, as in the constant and chemostat environments.
397 Unfortunately, there are no empirical studies comparing the benefits of aging versus repair in
398 biofilms, highlighting the dearth of studies of aging in the most common habitat of
399 microorganisms.
400
401 The evolved extent to which unicells segregate damage asymmetrically varies substantially
402 between species. This poses the question of whether this is due to differences in the
403 mechanism of cell growth and division, differences in the 'life span' of their habitats or the
404 degree to which these 'unicells' are actually multicellular with a clearer division of labor

between germline and soma. The budding yeast, *Saccharomyces cerevisiae,* was the first unicell shown to age (21) and, in fact, is the only unicell for which the evidence of aging under benign conditions, rather than as a stress response, remains strong (9, 20, 32–38, 74–77). Its habitat is very rich in sugars but short-lived (78), and we argued previously (46) that investing resources into repairing the cell rather than reproduction is less advantageous when the habitat is (reliably) transient. However, the fission yeast *Schizosaccharomyces pombe* lives in the same kind of habitat (79). Also, the bacterium *Caulobacter crescentus* lives attached to surfaces that are decaying or consumed by zooplankton and therefore similarly transient, yet the evidence for senescence in *C. crescentus* has dwindled since our 2014 publication (9, 34, 80). This suggests that our previously proposed explanation – that morphologically asymmetric cell division and high external mortality due to short-lived habitats are necessary and sufficient conditions to see aging in unicells – needs to be revised as these conditions appear necessary but not sufficient. A third condition, nascent multicellularity, needs to be also met, see below.

Recent studies of the fission yeast, following single cells for many generations, provide clear evidence that asymmetric damage segregation does not occur under benign conditions. Instead, it appears to be a stress response to deal with misfolded proteins, which aggregate and then fuse into fewer and larger aggregates, facilitating the segregation of the damage into one aged daughter cell with a reduced growth rate and higher mortality (32, 33, 81). Spivey *et al.* (2017) (37) found that cell death in the fission yeast was actually not preceded by the characteristics of aging. Nakaoka & Wakamoto (2017) (38) also found no increase of mortality with age, instead, they found mortality to increase with growth rate. Moreover, they found that aggregates can get lost from old pole cells during division so they can rejuvenate.

Remarkably, oxidative stress reduced growth rate only transiently and protein aggregates present in the cell after stress did not affect growth. Apart from fission yeast, a recent study of *C. crescentus* by Iyer-Biswas *et al.* (2014) (34) found a trend of decreasing fecundity over generations only at 37˚C, the highest temperature used. This could be considered a heat shock given typical lake temperatures where *C. crescentus* lives. Moreover, Schramm *et al.* (2019) (9) found no evidence for asymmetric segregation of protein aggregates, despite the morphologically asymmetric cell division in *C. crescentus*. In *E. coli*, the extent to which a cell segregates damage asymmetrically at division tends to increase with the severity of environmental stress that cells are exposed to (36). In *Mycobacterium tuberculosis*, segregation is critical for recovery from stress that resulted in damaged protein that cannot be repaired (35). An entirely different issue is survival during starvation, where aging has recently been proposed as an adaptive strategy based on the finding that starving *E. coli* cells, like non-starving humans, follow the Gompertz law of mortality (82). However, the Gompertz law has been shown to arise from a variety of processes, including tumor growth, growth of batch cultures and genetic or acquired susceptibilities to death (83–88), so no mechanistic conclusions can be drawn from finding that mortality follows the phenomenological Gompertz law.

Considering all evidence, the budding yeast appears to be the only studied 'unicell' where aging occurs in the absence of stress. However, neither its asymmetric cell division mechanism of budding, nor living in transient habitats, is sufficient to explain this difference. It seems to us that the common view of the budding yeast as a unicell may be mistaken and the missing ultimate reason why budding yeast ages is that it is, to some extent, a multicellular organism. First, the monophyletic yeast lineage (*Saccharomycotina*) is a branch of the *Ascomycota*, a

453 division of fungi that have many mycelial forms with multicellular hyphae, so yeasts have a
454 multicellular heritage (89). Second, yeast can easily evolve towards multicellularity when
455 cluster formation is selected (30, 31). Third, while many lab strains are mutants in a gene
456 required for filamentous growth, which would hamper genetic analysis, wild strains of yeast
457 are dimorphic with a unicellular yeast and a pseudohyphal multicellular form under starvation
458 (29). Thus, the 'unicellular' yeast is at the cusp of multicellularity. We propose that the
459 combination of the budding mechanism of asymmetric growth and division, dispersal
460 between transient habitats and nascent multicellularity are the ultimate reasons that the
461 budding yeast is the exception that evolved aging as part of the normal life cycle rather than
462 as a stress response.
463
464 Our study has several limitations. First, we have focused on the effect of damage on growth
465 rate rather than mortality. This is partly for simplicity and partly because some studies show
466 an increase of mortality with age (90) while others suggest mortality is random rather than
467 increasing with age (37, 38, 79). Second, we neglect damage that had not been repaired before
468 it became segregated or that would be prohibitively expensive to repair, since the work of Lin
469 Chao's group has covered this well. They showed that damage segregation under constant
470 environmental conditions leads to separate steady state levels of damage in old and young
471 lineage cells, meaning that growth rate and mortality of cells do not change over divisions (43,
472 44, 91–94). (Since there is no trend of deterioration and the replication of young and old
473 lineages do not fit a soma germline distinction, it is probably better to refer to this as damage
474 homeostasis rather than aging). Third, we avoided specific assumptions on mechanisms of
475 damage repair or segregation that are organism specific as these are subject to evolution and
476 our interest is the evolution of general strategies. Fourth, we have simplified the biofilm

477 system to growth on flat, inert surfaces without detachment. While our rough, finger like
478 biofilms capture typical aspects of biofilm structure, many processes and potential structures
479 could not be covered in this study as the number of possible combinations is huge.
480 Nonetheless, our study is the first to cover the extremes, from a perfectly mixed chemostat
481 to a simple biofilm without any mixing (no motility of cells and only diffusive transport of
482 substrate through boundary layer and biofilm). That the results were, surprisingly, essentially
483 the same for both extremes, suggests that the findings hold for environments in between
484 these extremes.
485
486 In conclusion, our model predictions are confirmed by the experimental literature showing
487 that aging provides fitness advantages only if the following necessary and sufficient conditions
488 are met in combination for a given organism: (i) presence of a cell division mechanism that
489 clearly enables asymmetric division of all damage such as budding; (ii) predominant habitat is
490 transient or the extrinsic mortality high for other reasons, favoring early reproduction; and
491 (iii) a degree of multicellularity is present. Otherwise, aging is advantageous only as a stress
492 response to deal with damage that failed to be repaired. Here, we have expanded the scope
493 of this prediction substantially from previous work in constant and dynamic but spatially
494 uniform environments by exploring biofilms as an exemplar of spatially structured systems
495 thought to harbor the majority of microbes in the environment. In contrast to our original
496 hypothesis, we found that repair is also better than damage segregation in biofilms.

MATERIALS AND METHODS

We are following the standard ODD (Overview, Design concepts, and Details) protocol for describing individual-based models to facilitate comparison and review (Grimm et al., 2006, 2010).

Purpose

The purpose of this study is to determine whether segregation or repair of damage is the optimal unicellular strategy for dealing with cellular damage in spatially structured systems such as biofilms. In order to do this, we expand upon our previous work in spatially uniform systems (constant and chemostat environments), Clegg *et al.* (2014) (46) by introducing a strategy for adaptive damage repair and further subdividing biomass into four rather than two components. All simulations described here were performed using the free and open-source modelling platform iDynoMiCS (individual-based Dynamics of Microbial Communities Simulator) (97).

State variables and scales

Growth parameters

Growth parameters (Table 1) used are for *Escherichia coli*, where available, and are the same as those used by Clegg *et al.* (2014) (46). Note that 'protein' is representative of the whole biomass.

517 TABLE 1 All symbols, variables and parameters used

Symbol	Name	Units
a	aging (damage accumulation) rate (constant)	0.1 h^{-1}
a'	aging rate proportional to net specific growth rate	dimensionless, 0.22
β	investment in repair as a proportion of the total protein (fixed)	dimensionless, 0.07
$\hat{\beta}$	adaptive investment in repair as a proportion of the total protein	dimensionless, between 0 and 1
μ_{max}	maximum specific growth rate (Koch & Wang, 1982)	1.2 h^{-1}
$\mu(S)$	specific growth rate as a function of substrate concentration	h^{-1}
K_S	Monod (half-saturation) constant (Koch & Wang, 1982)	0.00234 g L^{-1}
$P_{g,a}$	protein invested into growth, active	fg
$P_{r,a}$	protein invested into repair, active	fg
$P_{g,d}$	protein invested into growth, damaged	fg
$P_{r,d}$	protein invested into repair, damaged	fg
P_{act}	active protein ($P_{g,a} + P_{r,a}$)	fg
P_{dam}	damaged protein ($P_{g,d} + P_{r,d}$)	fg
P_{gro}	protein invested into growth ($P_{g,a} + P_{g,d}$)	fg
P_{rep}	protein invested into repair ($P_{r,a} + P_{r,d}$)	fg
P_{tot}	total protein ($P_{g,a} + P_{r,a} + P_{g,d} + P_{r,d} = P_{act} + P_{dam}$)	fg
P_{div}	threshold protein mass triggering division (46)	620 fg (dry mass)
Z	cellular age, or damaged protein as a proportion of total protein ($\frac{P_{dam}}{P_{tot}}$)	dimensionless, between 0 and 1
α	degree of asymmetry, or damage segregation	dimensionless, between 0 (fully symmetric) and 1 (fully asymmetric)
θ	baby mass fraction; proportion of protein inherited by the new pole cell (normally distributed with mean 0.5 and standard deviation 0.025)	dimensionless, between 0 and 1
Y_μ	growth yield, the efficiency of converting glucose to active protein (Neijssel *et al*., 1996)	0.444 g g^{-1}
Y_r	repair yield, the efficiency of converting damaged protein to active protein (46)	0.8 g g^{-1} (assumed)
$r(P_{act}, P_{dam})$	rate of repair	h^{-1}
S	substrate concentration	g L^{-1}
S_{in}	substrate concentration in the inflow (46) (used in the constant and chemostat environments)	0.00234 (constant) or

		0.00324 (chemostat) g L^{-1}
S_{bulk}	substrate concentration in the bulk liquid (used in the biofilm environment)	0.014222, 0.000889 or 0.003556 g L^{-1}
D	dilution rate (46)	0.3 (chemostat) or 0.6 (biofilm bulk liquid) h^{-1}
ρ	biomass density (dry mass); assumed to be lower in biofilms due to the presence of extracellular polymeric substances (EPS).	290 (constant and chemostat; (100)) or 201 (biofilm) g L^{-1} (assumed)
b_L	boundary layer thickness (unless otherwise stated)	48 µm (assumed)
δ^2	ratio of maximum substrate transport to maximum substrate consumption rate	dimensionless, 0.0017, 0.0069 or 0.028 (assumed)
σ_f	absolute deviation of biofilm front points from the mean front position; a measure of biofilm roughness	µm
h_{max}	maximum biofilm thickness (unless otherwise stated), above which cells would be removed (here, the simulation was stopped when this height was reached)	154 µm (assumed)
D_G	diffusivity of growth substrate (glucose)	6.7×10^{-10} m^2 s^{-1} (101)
S_f	shove factor (102)	1.10 (assumed)

Environments

Three environments were used for this study: constant, chemostat and biofilm.

Constant environment: Substrate concentration is kept constant and population size is kept to 1,000 as new cells randomly replace existing cells.

Chemostat environment: The simulation domain behaves like a chemostat of size 1 μm^3. A chemostat is a well-mixed system where fresh resources constantly flow in and cells and left-over resources constantly flow out, at the same dilution rate *D* (0.3 h^{-1}; Table 1).

526 *Biofilm environment:* Only two dimensional simulations were used, to simplify analysis,
527 however, the addition of a third dimension would not be expected to change results because
528 both horizontal dimensions are equivalent (68). The domain size is (256 x 256) μm^2, and the
529 spatial grid for solving the diffusion reaction equation has a resolution of (4 x 4) μm^2. The
530 glucose concentration in the bulk liquid connected to the biofilm domain is kept constant
531 throughout.
532
533 *Length of time simulated*
534 Constant and chemostat environment simulations were run for a maximum length of 500
535 days. Single species simulations were run for 500 days, and competition simulations were
536 stopped earlier if only one species remained in the simulation domain. Some single-species,
537 single-cell simulations were run for only three days when the purpose was to follow one old
538 pole cell over sufficient generations. Biofilm simulations were run until a maximum biofilm
539 height of 154 µm was reached.
540
541 Process overview and scheduling
542 *Growth, aging and repair*
543 Cell growth is exponential, as growth rate is proportional to the current mass of the cell (but
544 see about age dependence below). Cells divide once their total protein threshold, P_{div} (Table
545 1), is reached (randomized by drawing from a normal distribution with given mean ± standard
546 deviation; 0.5 ± 0.025). Cells are made of two types of biomass, referred to as protein: protein
547 invested into growth machinery, or protein invested into repair machinery, and protein may
548 be either active or damaged (Table 1). As cells grow, they make active protein that is invested
549 into growth. Active protein is damaged in one of two ways: at a constant rate (a), as in our

previous work (46), or at a rate that is proportional to the cellular specific growth rate (a'). If cells possess the ability to carry out repair, damaged protein is converted back to active protein, at a rate proportional to both the concentration of damaged protein and the concentration of active repair protein with rate constant β, but with an efficiency, or repair yield (Y_r), of 80% (these processes are summarized in Fig. 1).

Individuals can differ in their strategy for dealing with cellular damage, but strategies are inherited and do not evolve. There are two cell division strategies: cells either divide symmetrically or asymmetrically. Here we only look at complete symmetry or asymmetry as partial asymmetry always gave intermediate results in our previous study (46). In an asymmetrically dividing cell, the 'old pole' daughter cell inherits all damage (up to capacity), while the 'new pole' daughter cell inherits none and is therefore rejuvenated. There are three repair strategies: (i) No repair; (ii) Investing into repair machinery at a fixed fraction (β) of newly formed biomass. The optimal fixed fraction of investment as a function of damage accumulation rate was previously determined for chemostats (46); and (iii) Adaptive investment into repair machinery ($\hat{\beta}$) depending upon the current levels of damage within the cell. This adaptive repair strategy is new to studies that model aging and repair in unicells and was developed to account for the different specific growth rates of cells in a biofilm, which change in time and space. Altogether, there were six combinations of division and repair strategies used in this study (Fig. 1). All six combinations of division and repair strategies were used for initial, single-strategy investigations (*i.e.* Fig. 2), but only FR, AR and DS were used for competitions.

572 *Mortality (intrinsic and extrinsic)*

573 In all environments, cells may be considered dead when their age reaches 1, signifying that
574 there is no longer any active protein within the cell (intrinsic mortality). Such 'dead' cells are
575 assumed to remain physically intact and to continue to occupy space (only relevant for
576 biofilms) since cell wall degradation is presumably a slow process (taking many residence
577 times in the chemostat and longer than the times we simulate in biofilms).

578 *Constant environment:* a cell is removed at random each time a division occurs (extrinsic
579 mortality).

580 *Chemostat environment:* cells are removed randomly with the outflow from the chemostat at
581 the dilution rate (extrinsic mortality).

582 *Biofilm environment:* cells are not removed from the simulation for reasons given in the fitness
583 section (no extrinsic mortality). Rather than removing the cells when the maximum biofilm
584 height is reached (simulating detachment), we stop the simulation.

585

586 *Biofilm structure*

587 The formation of biofilm structure was investigated in the absence of aging and repair in order
588 to find conditions that would give typical biofilm structures, *e.g.* a smooth, an intermediate
589 and a rough biofilm. Earlier models have found that rougher and more finger-like biofilms tend
590 to be produced when nutrient availability is limiting growth (Picioreanu et al., 1998; Dockery
591 and Klapper, 2002; Olivera-Nappa et al., 2010). This can be achieved, *e.g.*, by reducing the
592 substrate concentration in the bulk liquid S_{bulk} or increasing the thickness of the boundary
593 layer b_L, which both have a direct effect on the flux with which substrate diffuses into the
594 biofilm, and therefore on the thickness of the actively growing layer (65). Dimensionless
595 groups have previously been introduced to explain the combined effects of S_{bulk} and b_L and

other parameters on biofilm structure (see the Supplementary Materials and Methods section for further explanation of these). Here we use:

$$\delta^2 = \frac{S_{bulk} D_G Y_\mu}{\mu_{max} \rho b_L^2}$$

where D_G is the diffusion coefficient of the growth substrate, Y_μ is the growth yield, μ_{max} is the maximal specific growth rate and ρ is the biomass density. In order to obtain biofilm structures that were smooth, intermediate or rough, b_L was kept constant at 48 μm and S_{bulk} took three different values (in g L^{-1}): 0.014222 (smooth, $\delta^2 = 0.028$), 0.003556 (intermediate, $\delta^2 = 0.0069$), and 0.000889 (rough, $\delta^2 = 0.0017$).

Time

Time is discrete. Since diffusion and biochemical reactions are on a faster timescale than growth and cell division, the diffusion-reaction equation is solved while the biomass distribution is fixed. Once the substrate concentration field is updated, it is kept fixed while the agents are stepped so they can grow and divide. Both diffusion-reaction and agent time steps were set to be the same at 0.01 h^{-1} in constant and chemostat environments, and 0.05 h^{-1} in biofilm environments where rates are lower.

Event scheduling

The simulation is entirely time stepped rather than event driven. The order in which agents are called in each time step is randomized.

Design concepts

Adaptation

Within this model, only those cells with the adaptive repair mechanism are able to adapt to their environment. These cells are able to sense their current cellular damage levels and invest into producing repair protein appropriately. Repair protein is assumed to be stable rather than turned over. In other words, repair protein is not converted back into growth protein if it is no longer needed.

Fitness

Fitness is an emergent property and not defined by a fitness function. In constant and chemostat environments, the fittest strategy is determined by competition as the only strategy remaining in the simulation domain. In biofilm simulations, the fittest strategy was determined by comparing population sizes, growth rates, and the log biomass ratio between the strategies. We have avoided detachment in these biofilm simulations as a metacommunity model would be required to simulate fitness as an emergent property when cells detach from a biofilm patch as other patches would need to be present for colonization by cells detached from the focal patch.

Observation

Data is written to xml files at user-defined intervals. This data includes the state of the environment, such as solute concentration fields, summary data on the population (*e.g.*, number of cells born or removed at each time step), as well as lists of individual cells with all of their properties, such as position, size, growth rate and investment into each protein type.

Since the entire state of all agents and the environment is saved, simulations can be restarted with this output.

Initialization

Environment

For the constant and chemostat environments, simulations are initiated with 1,000 cells (500 per strategy). Biofilm simulations are initiated with 4, 8, 16 or 32 cells (2, 4, 8 or 16, respectively, of each strategy), which are placed randomly on the substratum surface.

Input

Almost all system and agent parameters are specified in an xml input file called 'protocol' file. Example input files can be found at https://github.com/R-Wright-1/iDynoMiCS_1.5.

Sub-models

Mathematical skeleton

The following equations are for modeling growth, aging, and repair of individual cells. They are ordinary differential equations (ODEs). Their solution depends on conditions prescribed at one end of the interval of interest (Lick, 1989).

Individual Model Equations

The population is not modelled directly, but summary statistics are gathered and rates summed over all individuals. The substrate consumption rates of all individuals are gathered and summed and this total rate of substrate consumption enters the standard equation for

chemostat substrate dynamics (+ inflow − outflow − consumption). Note that the net specific growth rate of an individual is also the sum of the rates of change for all four components of the cell. We give the differential equations for the change of the cell's components below. Individuals do not have access to population level information and their behavior depends only on local conditions.

The biofilm environment consists of substrate concentration fields and a representation of the current biofilm structure (substratum surface, biofilm, biofilm boundary-layer interface and boundary-layer bulk-liquid interface). The environment is modelled as a continuum using partial differential equations (PDEs) to describe the diffusion of substrate and rates of substrate uptake (or product secretion) by the cells. For this purpose, the distributions of cellular masses and substrate consumption (reaction) rates are mapped to the grid used for solving the PDEs. The reaction diffusion PDEs are solved with a multigrid algorithm, see Lardon *et al.* (2011) (97) for more details.

Since adaptive repair has a variable fraction of repair machinery, the previously used P_{act} and P_{dam} have each to be split into two fractions:

$P_{g,a}$, $P_{r,a}$, $P_{g,d}$ and $P_{r,d}$, referring to growth machinery, active; repair machinery, active; growth machinery, damaged; and repair machinery, damaged, respectively (as in Table 1).

Thus, the total 'protein' of the cell (representing all biomass) is $P_{tot} = P_{g,d} + P_{r,d} + P_{g,a} + P_{r,a}$.

We assume that damage is always toxic, *i.e.*, specific growth rate, due to some inhibitory effect of damaged material, decreases with the fraction of damaged protein, Z, equivalent to the age of the cell:

$$Z = \frac{P_{g,d} + P_{r,d}}{P_{tot}}$$

Toxic damage led to more pronounced differences between the strategies in our previous study, whilst not changing the fitness ranking of strategies apart from one case, at the lowest damage accumulation rate and only in the constant environment, where the differences between strategies were minute (46).

In cells of all strategies, growth of active protein depends on substrate concentration *S* following Monod kinetics:

$$\mu(S) = \frac{\mu_{max}\, S}{K_S + S} \quad (1)$$

Where repair of damage takes place, the rate of repair is Michaelis-Menten like and proportional to damaged protein and active repair protein (see Clegg *et al.* (2014) (46) for further explanations):

$$r(P_{act}, P_{dam}) = \frac{\tilde{\beta}\, P_{act}\, P_{dam}}{\tilde{\beta}\, P_{act} + P_{dam}} \quad (2)$$

where $\tilde{\beta}\, P_{act}$ represents the proportion of active biomass that is dedicated to repairing damaged biomass and a placeholder for the value actually used depending on the repair strategy. For fixed repair, it becomes the fixed fraction β of active protein P_{act} that is repair machinery $\tilde{\beta}\, P_{act} = \beta\, P_{act}$. For adaptive repair, it is replaced by the currently active repair machinery $\tilde{\beta}\, P_{act} = P_{r,a}$, which is produced as a fraction of growth $\hat{\beta}$ calculated for each individual at every time step depending on its current fraction of damage (age Z) from the following equation:

$$\hat{\beta} = \left(\frac{Z}{1-Z}\right) max\left(\pm\sqrt{\frac{Y_r}{\mu(S)}\frac{1}{1-Z}} - 1\right) \quad (3)$$

which is the value of β that maximizes the rate of active protein production and is derived from $\frac{d(dP_{act}/dt)}{d\beta} = 0$.

For $\mu(S)$ in eq. 3, we do not take the gross specific growth rate according to eq. (1), but the net specific growth rate each individual cell calculates from its change of total mass from one iteration to the next, which due to inefficient repair could be less.

This gives the following differential equations for the four components of each individual cell for the case of toxic damage that is being repaired:

$$\frac{d}{dt}P_{g,a} = \left(1-\tilde{\beta}\right)\mu(S)\,P_{g,a}(1-Z) - A\,P_{g,a} + Y_r P_{r,a}\frac{P_{g,d}}{P_{r,a}+P_{r,d}} \quad (4a)$$

$$\frac{d}{dt}P_{r,a} = \tilde{\beta}\,\mu(S)\,P_{g,a}(1-Z) - A\,P_{r,a} + Y_r P_{r,a}\frac{P_{r,d}}{P_{r,a}+P_{r,d}} \quad (4b)$$

$$\frac{d}{dt}P_{g,d} = A\,P_{g,a} - P_{r,a}\frac{P_{g,d}}{P_{r,a}+P_{r,d}} \quad (4c)$$

$$\frac{d}{dt}P_{r,d} = A\,P_{r,a} - P_{r,a}\frac{P_{r,d}}{P_{r,a}+P_{r,d}} \quad (4d)$$

where A is a placeholder for the use of constant (a) or net specific growth rate proportional aging rate (a'):

$$a(\mu) = a'\,\frac{(dP_{tot}/dt)}{P_{tot}}$$

Cell division

Upon cell division, the post-division protein masses of the old pole cell are:

$$P_{a,g} = (1-\theta)P'_{a,g} - \alpha\theta P'_{d,g} \quad (5a)$$

$$P_{a,r} = (1-\theta)P'_{a,r} - \alpha\theta P'_{d,r} \quad (5b)$$

$$P_{d,g} = (1-\theta)P'_{d,g} + \alpha\theta P'_{d,g} \quad (5c)$$

$$P_{d,r} = (1-\theta)P'_{d,r} + \alpha\theta P'_{d,r} \quad (5d)$$

and those of the new pole cell are:

$$P_{a,g} = \theta P'_{a,g} + \alpha\theta P'_{d,g} \quad (6a)$$

$$P_{a,r} = \theta P'_{a,r} + \alpha\theta P'_{d,r} \quad (6b)$$

$$P_{d,g} = \theta P'_{d,g} - \alpha\theta P'_{d,g} \quad (6c)$$

730 $$P_{d,r} = \theta P'_{d,r} - \alpha\theta P'_{d,r} \quad (6d)$$

731 where the prime indicates the protein amounts in the pre-division cell, θ the proportion of
732 protein inherited by the new pole cell and α the asymmetry of cell division ($\alpha = 1$ fully
733 asymmetric division, $\alpha = 0$ fully symmetric division). However, if there is more damage than
734 the old pole daughter cell can take (when $(1-\theta)P'_{a,g} < \alpha\theta P'_{d,g}$ *or* $(1-\theta)P'_{a,r} < \alpha\theta P'_{d,r}$
735 so the old pole-cell would inherit a negative quantity of active protein following eq. 5), the old
736 pole cell is assumed to be filled with damaged protein:

737 $$P_{a,g} = 0 \quad (7a)$$

738 $$P_{a,r} = 0 \quad (7b)$$

739 $$P_{d,g} = (1-\theta)(P'_{a,g} + P'_{d,g}) \quad (7c)$$

740 $$P_{d,r} = (1-\theta)(P'_{a,r} + P'_{d,r}) \quad (7d)$$

741 and the new pole cell inherits all of the active protein, plus the remainder of the damaged
742 protein:

743 $$P_{a,g} = P'_{a,g} \quad (8a)$$

744 $$P_{a,r} = P'_{a,r} \quad (8b)$$

745 $$P_{d,g} = \theta P'_{d,g} - (1-\theta)P'_{a,g} \quad (8c)$$

746 $$P_{d,r} = \theta P'_{d,r} - (1-\theta)P'_{a,r} \quad (8d)$$

747

748 *Aging*

749 The growth independent aging rate of 0.1 h^{-1}, used in Clegg et al. (2014), was suitable for
750 constant and chemostat (spatially uniform steady state) environments, but was not suitable
751 for biofilm (spatially structured) environments. Most cells within biofilms are not actively
752 growing. Only those cells in the top or active layer of biofilms have access to substrate and are
753 actively growing. It therefore makes sense to assume that non-growing cells that do not

produce proteins or respire do not accumulate damage (19, 71, 72). Thus, the damage accumulation rate was assumed to be proportional to cellular specific growth rate.

In order to compare strategies across environments, we need to apply the same damage accumulation rate in all three environments. Hence, the new damage accumulation rate that is proportional to specific growth rate, a', must be calculated to match the fixed damage accumulation rate in the spatially uniform environments ($a = 0.1$ h^{-1}) where the specific growth rate is constant or predictable for a steady state. In the steady state of the chemostat, the net specific growth rate, μ_N, is equal to the dilution rate, D, which was set to 0.3 h^{-1}. In iDynoMiCS, the gross specific growth rate, μ_G, is calculated with the Monod equation and depends on substrate concentration, S. However, how much the net specific growth rate is lower than the gross specific growth rate depends on the age of the cell, its rate of repair and its current level of investment into repair. It is therefore difficult to work out analytically so we had to run a number of simulations with different ratios of aging rates to specific growth rates to find that a value of 0.22 (dimensionless) would match the previously used constant aging rate for chemostats (Fig. S6).

Diagram of processes

A diagram containing a brief overview of all cellular processes is in Fig. 1.

iDynoMiCS Simulations

Cell strategies

Six combinations of damage segregation and repair strategies were used in this study, but only the fittest three of these were used in biofilm simulations: asymmetric division without repair (DS), symmetric division with adaptive repair (AR), and symmetric division with fixed repair

778 (FR). They are described in the schematic depicted in Fig. 1. Damage is considered to be toxic
779 in all simulations as toxic damage leads to greater differences between strategies (46).
780
781 *Comparison with previous fixed repair*
782 In order to compare the new, adaptive repair strategy developed here with the previous fixed
783 repair (as in (46), single strategy and competition simulations were run in iDynoMiCS. These
784 simulations were initiated with 1,000 cells for single strategies or 500 of each strategy for
785 competitions. The single strategy simulations were run for 3 days in the constant
786 environment, where the 'old pole' cell was artificially kept in the simulation, rather than
787 allowing random removal, to examine the consequences of adaptive repair on an individual
788 cell (Fig. 2). Alternatively, they were run for 500 days, to examine the consequences of
789 adaptive repair on populations of cells. Competitions between cells of different strategies
790 were run in both the constant and chemostat environments for a maximum of 500 days, or
791 until only one strategy remained in the simulation domain (n=10 for each).
792
793 *Biofilm environment simulations*
794 We initially carried out biofilm simulations with a single strategy without aging or repair to
795 determine the parameters that would give rise to typical biofilm structures. For these, cells
796 were initially placed evenly on the substratum surface. For all further simulations, with
797 damage accumulation and repair, cells were initially placed at random on the substratum
798 surface.
799

800 **Software and hardware used**

801 iDynoMiCS 1.5 is free open source software written in Java (46, 97). Analysis scripts were

802 written in Python 2.7.10 (Python Software Foundation, 2010). All source and analysis code can

803 be found at https://github.com/R-Wright-1/iDynoMiCS_1.5.

804

Supplemental Material

- Supplementary file containing Figures S1-S7, Table S1 and Supplementary Materials and Methods.
- **File S1.** Uploaded to Figshare: https://doi.org/10.6084/m9.figshare.11520534.v1. Includes further supplementary figures with biofilm plots for all biofilm simulations performed.

REFERENCES

1. Healy K, Guillerme T, Finlay S, Kane A, Kelly SBA, Mcclean D, Kelly J, Donohue I, Jackson AL, Cooper N, B PRS, Kelly BA, Kelly DJ. 2014. Ecology and mode-of-life explain lifespan variation in birds and mammals. Proc R Soc B 281.
2. Jones OR, Scheuerlein A, Salguero-Gómez R, Camarda CG, Schaible R, Casper BB, Dahlgren JP, Ehrlén J, García MB, Menges ES, Quintana-Ascencio PF, Caswell H, Baudisch A, Vaupel JW. 2014. Diversity of ageing across the tree of life. Nature 505:169–173.
3. Florea M. 2017. Aging and immortality in unicellular species. Mech Ageing Dev 167:5–15.
4. Kirkwood TBL, Cremer T. 1982. Cytogerontology Since 1881: A Reappraisal of August Weismann and a Review of Modern Progress. Hum Genet 60:101–121.
5. Kirkwood TBL. 2005. Understanding the odd science of aging. Cell 120:437–447.
6. Stewart EJ, Madden R, Paul G, Taddei FF. 2005. Aging and death in an organism that reproduces by morphologically symmetric division. PLoS Biol 3:0295–0300.
7. Ackermann M, Stearns SC, Jenal U. 2003. Senescence in a bacterium with asymmetric division. Science (80-) 300:1920.
8. Iyer-Biswas S, Wright CS, Henry JT, Lo K, Burov S, Lin Y, Crooks GE, Crosson S, Dinner AR, Scherer NF. 2014. Scaling laws governing stochastic growth and division of single bacterial cells. Proc Natl Acad Sci U S A 111:15912–7.
9. Schramm FD, Schroeder K, Alvelid J, Testa I, Jonas K. 2019. Growth-driven displacement of protein aggregates along the cell length ensures partitioning to both daughter cells in Caulobacter crescentus. Mol Microbiol 111:1430–1448.
10. Stewart EJ, Madden R, Paul G, Taddei F. 2005. Aging and death in an organism that reproduces by morphologically symmetric division. PLoS Biol 3:0295–0300.
11. Lindner AB, Madden R, Demarez A, Stewart EJ, Taddei F. 2008. Asymmetric segregation of protein aggregates is associated with cellular aging and rejuvenation. Proc Natl Acad Sci 105:3076–3081.
12. Barker MG, Walmsley RM. 1999. Replicative ageing in the fission yeast Schizosaccharomyces pombe. Yeast 15:1511–1518.
13. Veening J-W, Stewart EJ, Berngruber TW, Taddei F, Kuipers OP, Hamoen LW. 2008. Bet-hedging and epigenetic inheritance in bacterial cell development. Proc Natl Acad Sci 105:4393–4398.
14. Aldridge BB, Fernandez-Suarez M, Heller D, Ambravaneswaran V, Irimia D, Toner M, Fortune SM. 2012. Asymmetry and Aging of Mycobacterial Cells Lead to Variable Growth and Antibiotic Susceptibility. Science (80-) 335:100–104.
15. Bergmiller T, Ackermann M. 2011. Pole age affects cell size and the timing of cell division in Methylobacterium extorquens AM1. J Bacteriol 193:5216–5221.
16. Laney SR, Olson RJ, Sosik HM. 2012. Diatoms favor their younger daughters. Limnol Oceanogr 57:1572–1578.
17. Humby PL, Snyder ECR, Durnford DG. 2013. Conditional senescence in Chlamydomonas reinhardtii (Chlorophyceae). J Phycol 49:389–400.
18. Damodaran SP, Eberhard S, Boitard L, Rodriguez JG, Wang Y, Bremond N, Baudry J, Bibette J, Wollman FA. 2015. A millifluidic study of cell-to-cell heterogeneity in growth-rate and cell-division capability in populations of isogenic cells of Chlamydomonas reinhardtii. PLoS One 10:1–28.

19. Moger-Reischer RZ, Lennon JT. 2019. Microbial ageing and longevity. Nat Rev Microbiol 17:679–690.
20. Wang L, Schubert D, Sawaya MR, Eisenberg D, Riek R. 2010. Multidimensional structure-activity relationship of a protein in its aggregated states. Angew Chemie - Int Ed 49:3904–3908.
21. Mortimer RK, Johnston JR. 1959. Life Span of Individual Yeast Cells. Nature 183:1751–1752.
22. Crane MM, Clark IBN, Bakker E, Smith S, Swain PS. 2014. A microfluidic system for studying ageing and dynamic single-cell responses in budding yeast. PLoS One 9:1–10.
23. Jo MC, Liu W, Gu L, Dang W, Qin L. 2015. High-throughput analysis of yeast replicative aging using a microfluidic system. Proc Natl Acad Sci 112:9364–9369.
24. Kaya A, Lobanov A V., Gladyshev VN. 2015. Evidence that mutation accumulation does not cause aging in Saccharomyces cerevisiae. Aging Cell 14:366–371.
25. Saarikangas J, Barral Y. 2015. Protein aggregates are associated with replicative aging without compromising protein quality control. Elife 4:1–24.
26. Paoletti C, Quintin S, Matifas A, Charvin G. 2016. Kinetics of Formation and Asymmetrical Distribution of Hsp104-Bound Protein Aggregates in Yeast. Biophys J 110:1605–1614.
27. Sarnoski EA, Song R, Ertekin E, Koonce N, Acar M. 2018. Fundamental Characteristics of Single-Cell Aging in Diploid Yeast. iScience 7:96–109.
28. Yang J, McCormick MA, Zheng J, Xie Z, Tsuchiya M, Tsuchiyama S, El-Samad H, Ouyang Q, Kaeberlein M, Kennedy BK, Li H. 2015. Systematic analysis of asymmetric partitioning of yeast proteome between mother and daughter cells reveals “aging factors” and mechanism of lifespan asymmetry. Proc Natl Acad Sci U S A 112:11977–11982.
29. Kron SJ. 1997. Filamentous growth in budding yeast. Trends Microbiol 5:450–454.
30. Ratcliff WC, Denison RF, Borrello M, Travisano M. 2012. Experimental evolution of multicellularity. Proc Natl Acad Sci 109:1595–1600.
31. Ratcliff WC, Fankhauser JD, Rogers DW, Greig D, Travisano M. 2015. Origins of multicellular evolvability in snowflake yeast. Nat Commun 6:1–9.
32. Coelho M, Dereli A, Haese A, Kühn S, Malinovska L, Desantis ME, Shorter J, Alberti S, Gross T, Tolić- IM. 2013. Fission yeast does not age under favorable conditions, but does so after stress. Curr Biol 23:1844–1852.
33. Coelho M, Lade SJ, Alberti S, Gross T, Tolić IM. 2014. Fusion of Protein Aggregates Facilitates Asymmetric Damage Segregation. PLoS Biol 12:1–11.
34. Iyer-Biswas S, Wright CS, Henry JT, Lo K, Burov S, Lin Y, Crooks GE, Crosson S, Dinner AR, Scherer NF. 2014. Scaling laws governing stochastic growth and division of single bacterial cells. Proc Natl Acad Sci 111:15912–15917.
35. Vaubourgeix J, Lin G, Dhar N, Chenouard N, Jiang X, Botella H, Lupoli T, Mariani O, Yang G, Ouerfelli O, Unser M, Schnappinger D, McKinney J, Nathan C. 2015. Stressed mycobacteria use the chaperone ClpB to sequester irreversibly oxidized proteins asymmetrically within and between cells. Cell Host Microbe 17:178–190.
36. Vedel S, Nunns H, Košmrlj A, Semsey S, Trusina A. 2016. Asymmetric Damage Segregation Constitutes an Emergent Population-Level Stress Response. Cell Syst 3:187–198.
37. Spivey EC, Jones SK, Rybarski JR, Saifuddin FA, Finkelstein IJ. 2017. An aging-independent replicative lifespan in a symmetrically dividing eukaryote. Elife 6:1–25.

905 38. Nakaoka H, Wakamoto Y. 2017. Aging, mortality, and the fast growth trade-off of
906 Schizosaccharomyces pombe. PLoS Biol 15:1–29.
907 39. Watve M, Parab S, Jogdand P, Keni S. 2006. Aging may be a conditional strategic
908 choice and not an inevitable outcome for bacteria. Proc Natl Acad Sci U S A
909 103:14831–5.
910 40. Erjavec N, Cvijovic M, Klipp E, Nystrom T. 2008. Selective benefits of damage
911 partitioning in unicellular systems and its effects on aging. Proc Natl Acad Sci
912 105:18764–18769.
913 41. Rashidi A, Kirkwood TBL, Shanley DP. 2012. Aging Research in Yeast 57:315–330.
914 42. Medawar PB. 1951. An Unsolved Problem of Biology. H. K. Lewis & Co Ltd London.
915 43. Chao L. 2010. A model for damage load and its implications for the evolution of
916 bacterial aging. PLoS Genet 6:e1001076.
917 44. Proenca AM, Rang CU, Buetz C, Shi C, Chao L. 2018. Age structure landscapes emerge
918 from the equilibrium between aging and rejuvenation in bacterial populations. Nat
919 Commun 9.
920 45. Ackermann M, Schauerte A, Stearns SC, Jenal U. 2007. Experimental evolution of
921 aging in a bacterium. BMC Evol Biol 7:1–10.
922 46. Clegg RJ, Dyson RJ, Kreft J-U. 2014. Repair rather than segregation of damage is the
923 optimal unicellular aging strategy. BMC Biol 12:52.
924 47. Collins S. 2016. Growth rate evolution in improved environments under Prodigal Son
925 dynamics. Evol Appl 9:1179–1188.
926 48. Song R, Acar M. 2019. Stochastic modeling of aging cells reveals how damage
927 accumulation, repair, and cell-division asymmetry affect clonal senescence and
928 population fitness. BMC Bioinformatics 20:1–14.
929 49. Costerton JW, Lewandowski Z, Caldwell DE, Korber DR, Lappin-Scott HM. 1995.
930 Microbial biofilms. Annu Rev Microbiol 711–745.
931 50. Eberl HJ, Parker DF, Van Loosdrecht MCM. 2001. A New Deterministic Spatio-
932 Temporal Continuum Model for Biofilm Development. J Theor Med 3:161–175.
933 51. Stewart PS. 2003. Diffusion in Biofilms. J Bacteriol 185:1485–1491.
934 52. Hall CW, Mah TF. 2017. Molecular mechanisms of biofilm-based antibiotic resistance
935 and tolerance in pathogenic bacteria. FEMS Microbiol Rev 41:276–301.
936 53. Flemming H-C, Wingender J, Szewzyk U, Steinberg P, Rice SA, Kjelleberg S. 2016.
937 Biofilms: an emergent form of bacterial life. Nat Rev Microbiol 14:563–575.
938 54. Hall-Stoodley L, Costerton JW, Stoodley P, State M, Engineering B. 2004. Bacterial
939 biofilms: from the natural environment to infectious diseases. Nat Rev Microbiol
940 2:95–108.
941 55. Dang H, Lovell CR. 2000. Bacterial primary colonization and early succession on
942 surfaces in marine waters as determined by amplified rRNA gene restriction analysis
943 and sequence analysis of 16S rRNA genes. Appl Environ Microbiol 66:467–475.
944 56. Davey ME, O'Toole GA. 2000. Microbial biofilms: from ecology to molecular genetics.
945 Microbiol Mol Biol Rev 64:847–67.
946 57. Tolker-Nielsen T, Brinch UC, Ragas PC, Andersen JB, Jacobsen CS, Molin S. 2000.
947 Development and dynamics of Pseudomonas sp. biofilms. J Bacteriol 182:6482–6489.
948 58. Picioreanu C, Kreft JU, Klausen M, Haagensen JAJ, Tolker-Nielsen T, Molin S. 2007.
949 Microbial motility involvement in biofilm structure formation - A 3D modelling study.
950 Water Sci Technol 55:337–343.
951 59. Ghanbari A, Dehghany J, Schwebs T, Müsken M, Häussler S, Meyer-Hermann M. 2016.

Inoculation density and nutrient level determine the formation of mushroom-shaped structures in Pseudomonas aeruginosa biofilms. Sci Rep 6:1–12.

60. Nadell CD, Drescher K, Foster KR. 2016. Spatial structure, cooperation and competition in biofilms. Nat Rev Microbiol 14:589–600.
61. Kirkwood TBL. 2005. Asymmetry and the origins of ageing. Mech Ageing Dev 126:533–534.
62. Christiano R, Nagaraj N, Fröhlich F, Walther TC. 2014. Global Proteome Turnover Analyses of the Yeasts S.cerevisiae and S.pombe. Cell Rep 9:1959–1966.
63. Picioreanu C, van Loosdrecht M, Heijnen J. 1998. Mathematical Modeling of Biofilm Strucutre with a Hybrid Differential-Discrete Cellular Automata Approach. Biotechnol Bioeng 58:101–116.
64. Dockery J, Klapper I. 2002. Finger Formation in Biofilm Layers. Siam J Appl Math 62:853–869.
65. Nadell CD, Foster KR, Xavier JB. 2010. Emergence of spatial structure in cell groups and the evolution of cooperation. PLoS Comput Biol 6.
66. Alpkvist E, Klapper I. 2007. Description of mechanical response including detachment using a novel particle model of biofilm/flow interaction. Water Sci Technol 55:265–273.
67. Kreft JU, Picioreanu C, Wimpenny JW, van Loosdrecht MC. 2001. Individual-based modelling of biofilms. Microbiology 147:2897–912.
68. Picioreanu C, Kreft J, Van MCM, Loosdrecht MCM Van. 2004. Particle-Based Multidimensional Multispecies Biofilm Model Particle-Based Multidimensional Multispecies Biofilm Model. Appl Environ Microbiol 70:3024–3040.
69. Picioreanu C, Blauert F, Horn H, Wagner M. 2018. Determination of mechanical properties of biofilms by modelling the deformation measured using optical coherence tomography. Water Res 145:588–598.
70. So M, Terashima M, Goel R, Yasui H. 2015. Modelling the Effect of Biofilm Morphology on Detachment. J Water Environ Technol 13:49–62.
71. Gladyshev VN. 2014. The free radical theory of aging is dead. Long live the damage theory! Antioxidants Redox Signal 20:727–731.
72. Ogrodnik M, Salmonowicz H, Gladyshev VN. 2019. Integrating cellular senescence with the concept of damage accumulation in aging: Relevance for clearance of senescent cells. Aging Cell 18:1–21.
73. Lee WS, Monaghan P, Metcalfe NB. 2013. Experimental demonstration of the growth rate-lifespan trade-off. Proc R Soc B Biol Sci 280.
74. Zhou C, Li R, Kennedy BK. 2014. Life history: Mother-specific proteins that promote aging. Curr Biol 24:R1162–R1164.
75. Zhou C, Slaughter BD, Unruh JR, Guo F, Yu Z, Mickey K, Narkar A, Ross RT, McClain M, Li R. 2014. Organelle-based aggregation and retention of damaged proteins in asymmetrically dividing cells. Cell 159:530–542.
76. Coelho M. 2015. Aging and stress The role of the environment in cellular replication. Longevity 4–7.
77. Thayer NH, Leverich CK, Fitzgibbon MP, Nelson ZW, Henderson KA, Gafken PR, Hsu JJ, Gottschling DE. 2014. Identification of long-lived proteins retained in cells undergoing repeated asymmetric divisions. Proc Natl Acad Sci 111:14019–14026.
78. Stefanini I, Dapporto L, Legras J-L, Calabretta A, Di Paola M, De Filippo C, Viola R, Capretti P, Polsinelli M, Turillazzi S, Cavalieri D. 2012. Role of social wasps in

999 Saccharomyces cerevisiae ecology and evolution. Proc Natl Acad Sci 109:13398–
1000 13403.
1001 79. Coelho M, Dereli A, Haese A, Kühn S, Malinovska L, Desantis ME, Shorter J, Alberti S,
1002 Gross T, Tolić-Nørrelykke IM. 2013. Fission yeast does not age under favorable
1003 conditions, but does so after stress. Curr Biol 23:1844–1852.
1004 80. Wright C, Iyer-Biswas S. 2016. Aging of Individual Cells Over Tens of Generations.
1005 Biophys J 110:144a-145a.
1006 81. Lade SJ, Coelho M, Tolić IM, Gross T. 2015. Fusion leads to effective segregation of
1007 damage during cell division: An analytical treatment. J Theor Biol 378:47–55.
1008 82. Yang Y, Santos AL, Xu L, Lotton C, Taddei F, Lindner B. 2019. Temporal scaling of
1009 ageing as an adaptive strategy of Escherichia coli.
1010 83. Yashin AI, Vaupel JW, Iachine IA. 1994. A duality in aging: the equivalence of mortality
1011 models based on radically different concepts. Mech Ageing Dev 74:1–14.
1012 84. Benzekry S, Lamont C, Beheshti A, Tracz A, Ebos JML, Hlatky L, Hahnfeldt P. 2014.
1013 Classical Mathematical Models for Description and Prediction of Experimental Tumor
1014 Growth. PLoS Comput Biol 10.
1015 85. Kogan V, Molodtsov I, Menshikov LI, Reis RJS, Fedichev P. 2015. Stability analysis of a
1016 model gene network links aging, stress resistance, and negligible senescence. Sci Rep
1017 5:1–12.
1018 86. Santra M, Dill KA, De Graff AMR. 2019. Proteostasis collapse is a driver of cell aging
1019 and death. Proc Natl Acad Sci U S A 116:22173–22178.
1020 87. Sarapata EA, de Pillis LG. 2013. A Comparison and Catalog of Intrinsic Tumor Growth
1021 Models. arXiv:13124857.
1022 88. Zwietering MH, Jongenburger I, Rombouts FM, Riet KV. 1990. Modeling of the
1023 Bacterial Growth Curve. Appl Environ Microbiol 56:1875–1881.
1024 89. Paleo-López R, Quintero-Galvis JF, Solano-Iguaran JJ, Sanchez-Salazar AM, Gaitan-
1025 Espitia JD, Nespolo RF. 2016. A phylogenetic analysis of macroevolutionary patterns in
1026 fermentative yeasts. Ecol Evol 6:3851–3861.
1027 90. Wang P, Robert L, Pelletier J, Dang WL, Taddei F, Wright A, Jun S. 2010. Robust growth
1028 of Escherichia coli. Curr Biol 20:1099–1103.
1029 91. Chao L, Rang CU, Proenca AM, Chao JU. 2016. Asymmetrical Damage Partitioning in
1030 Bacteria: A Model for the Evolution of Stochasticity, Determinism, and Genetic
1031 Assimilation. PLoS Comput Biol 12:1–17.
1032 92. Proenca AM, Rang CU, Qiu A, Shi C, Chao L. 2019. Cell aging preserves cellular
1033 immortality in the presence of lethal levels of damage. PLoS Biol 17:1–21.
1034 93. Rang CU, Peng AY, Chao L. 2011. Temporal dynamics of bacterial aging and
1035 rejuvenation. Curr Biol 21:1813–1816.
1036 94. Rang CU, Peng AY, Poon AF, Chao L. 2012. Ageing in Escherichia coli requires damage
1037 by an extrinsic agent. Microbiol (United Kingdom) 158:1553–1559.
1038 95. Grimm V, Berger U, Bastiansen F, Eliassen S, Ginot V, Giske J, Goss-Custard J, Grand T,
1039 Heinz SK, Huse G, Huth A, Jepsen JU, Jørgensen C, Mooij WM, Müller B, Pe'er G, Piou
1040 C, Railsback SF, Robbins AM, Robbins MM, Rossmanith E, Rüger N, Strand E, Souissi S,
1041 Stillman RA, Vabø R, Visser U, DeAngelis DL. 2006. A standard protocol for describing
1042 individual-based and agent-based models. Ecol Modell 198:115–126.
1043 96. Grimm V, Berger U, DeAngelis DL, Polhill JG, Giske J, Railsback SF. 2010. The ODD
1044 protocol: A review and first update. Ecol Modell 221:2760–2768.
1045 97. Lardon LA, Merkey B V, Martins S, Dötsch A, Picioreanu C, Kreft J-U, Smets BF. 2011.

iDynoMiCS: next-generation individual-based modelling of biofilms. Environ Microbiol 13:2416–34.

98. Koch A, Wang C. 1982. How close to the theoretical diffusion limit do bacterial uptake systems function? Arch Microbiol 36–42.
99. Neijssel OM, Teixeira De Mattos MJ, Tempest DW. 1996. Growth yield and energy distribution. Escherichia coli Salmonella, Cell Mol Biol by F Niedhart 2:1683–1693.
100. Shuler ML, Leung S, Dick CC. 1979. A Mathematical Model for the Growth of a Single Bacterial Cell. Ann N Y Acad Sci 326:35–52.
101. Goldberg RN, Tewari YB. 1989. Thermodynamic and Transport Properties of Carbohydrates and their Monophosphates: The Pentoses and Hexoses. J Phys Chem Ref Data 18:809–880.
102. Clegg RJ, Kreft JU. 2017. Reducing discrepancies between 3D and 2D simulations due to cell packing density. J Theor Biol 423:26–30.
103. Olivera-Nappa A, Picioreanu C, Asenjo JA. 2010. Non-homogeneous biofilm modeling applied to bioleaching processes. Biotechnol Bioeng 106:660–676.
104. Lick WJ. 1989. Ordinary Differential Equations. Springer Berlin Heidelberg, Berlin, Heidelberg.